Sequential doping of solid chunks of a conjugated polymer for body-heat-powered thermoelectric modules

(article starts on next page)

Sequential doping of solid chunks of a conjugated polymer for body-heat-powered thermoelectric modules

Liyang Yu, [iD] Dorothea Scheunemann, Anja Lund, et al.

COLLECTIONS

Paper published as part of the special topic on Organic and Hybrid Thermoelectrics

View Online   Export Citation   CrossMark

ARTICLES YOU MAY BE INTERESTED IN

Applied Physics Letters

Sequential doping of solid chunks of a conjugated polymer for body-heat-powered thermoelectric modules

Liyang Yu,[1,2,a)] Dorothea Scheunemann,[2] Anja Lund,[2] David Kiefer,[2] and Christian Müller[2,a)]

AFFILIATIONS

[1]School of Chemical Engineering, Sichuan University, Chengdu 610064, People's Republic of China
[2]Department of Chemistry and Chemical Engineering, Chalmers University of Technology, 41296 Gothenburg, Sweden

Note: This paper is part of the APL Special Collection on Organic and Hybrid Thermoelectrics.
[a)]Authors to whom correspondence should be addressed: liyangyu@scu.edu.cn and christian.muller@chalmers.se

ABSTRACT

Sequential doping of 1 mm³ sized cubes of regio-regular poly(3-hexylthiophene) (P3HT) with 2,3,5,6-tetrafluoro-tetracyanoquinodimethane is found to result in a doping gradient. The dopant ingresses into the solid material and after two weeks of sequential doping yields a 250 μm thick doped surface layer, while the interior of the cubes remains undoped. The doping gradient is mapped with energy dispersive x-ray spectroscopy (EDX), which is used to estimate a diffusion coefficient of 1×10^{-10} cm² s⁻¹ at room temperature. The cubes, prepared by pressing at 150 °C, feature alignment of polymer chains along the flow direction, which yields an electrical conductivity of 2.2 S cm⁻¹ in the same direction. A 4-leg thermoelectric module was fabricated with slabs of pressed and doped P3HT, which generated a power of 0.22 μW for a temperature gradient of 10.2 °C generated by body heat.

Thermoelectric devices, which convert heat directly into electricity, are an intriguing complement to other energy-harvesting technologies, such as solar cells for powering the myriad of distributed devices that will make up tomorrow's *Internet of Things*.[1–3] Conjugated polymers currently receive considerable attention in the context of thermoelectric devices because they offer a number of advantages, such as cost-effective processing from solution or melt as well as a superior mechanical flexibility and ductility compared to inorganic semiconductors. Moreover, polymeric materials offer a low thermal conductivity (κ), which makes them interesting candidates for the design of thermoelectric devices that can harvest low-grade heat sources, such as body heat.[4–6] Typically, the thermoelectric performance of materials is evaluated using a dimensionless figure of merit:

$$zT = \frac{\alpha^2 \sigma}{\kappa} T, \quad (1)$$

where α is the Seebeck coefficient, σ is the electrical conductivity, and T is the absolute temperature.

A polymer semiconductor must be doped to obtain a thermoelectric material. A redox dopant is added to the polymer semiconductor, and electron transfer between the two molecules creates charges on the polymer backbone. Charge transport and, hence, the electrical conductivity strongly depend on the degree of order of the polymer, and hence, it is important that doping does not unduly disrupt the nano- and microstructure. For many polymers, the highest conductivity and thermoelectric power factor $\alpha^2 \sigma$ are obtained when the polymer is first processed from solution or melt, followed by a second doping step. Such sequential doping can be done by bringing the solidified polymer in contact with a dopant solution[7,8] or by exposing the polymer to dopant vapor.[9,10] For example, Brinkmann *et al.* have shown that in-plane alignment of about 50 nm thin polymer films followed by sequential doping can result in power factors as high as 2 mW m⁻¹ K⁻².[11]

The time required to fully dope a solid material depends on its dimensions. The widely used dopant 2,3,5,6-tetrafluoro-tetracyanoquinodimethane (F4TCNQ) has a diffusion coefficient of about 10^{-11} cm² s⁻¹ at room temperature in thin films of polymers, such as poly(3-hexylthiophene) (P3HT) and poly(2,5-bis(3-alkylthiophen-2-yl)thieno[3,2-*b*]thiophene) (PBTTT).[12,13] As a result, sequential doping proceeds slowly and it can be expected that doping of thick samples will take an excessively long time. This poses a challenge since

the legs of a thermoelectric module must be up to several millimeters thick so that the thermal gradient between heat source and sink leads to an appreciable temperature difference across the device.[4,14]

We were interested in assessing to what extent it is possible to dope the interior of solid chunks of a conjugated polymer through sequential doping. P3HT with a weight-average molecular weight of $M_w \sim 106$ kg mol^{-1} (regio-regularity $\sim$95%, polydispersity index ~ 1.65) was pressed into rectangular blocks at 150 °C using a channel die (see supplementary material for details), which resulted in alignment of polymer chains along the flow direction.[15] P3HT cubes that were $1 \times 1 \times 1$ mm^3 in size were cut from the pressed blocks and placed in a saturated solution of F4TCNQ in dichloromethane:acetonitrile (1:1 volume ratio) at room temperature [Fig. 1(a)]. P3HT cubes remained in the dopant solution for 14 days, protected from light. Sequential doping resulted in a decrease in density from $\rho = 1.01$ to 0.96 g cm^{-3} and in specific heat capacity from $C_p = 1.3$ to 1.0 J kg^{-1} K^{-1}. Doped cubes were immediately cut along three different planes as illustrated in Fig. 1(a). The direction of the material flow in the channel die, the direction along which the load was applied, and the third axis (normal to the channel die walls) are referred to as x, y, and z, respectively.

The exposed cross sections were at once examined with scanning electron microscopy (SEM) [Fig. 1(b)]. Energy dispersive x-ray spectroscopy (EDX) allowed us to map the intensity of the fluorine signal as a function of distance from the surface of the cubes from which the dopant had diffused into the polymer [Figs. 1(b) and 2(a)]. As illustrated in Fig. 1, from the cross section cut perpendicular to the y-axis, dopant ingression along the x- and z-axes can be examined. Evidently, the evolution of the dopant concentration along the two axes follows clear "U" shape profiles with the highest dopant content at the surface

of the cube (position $= 0 \mu$m) and no discernable fluorine signal at the center of the block [see Fig. 2(a)]. The doped region extended around 250 μm from the surfaces of the cube into the bulk. Similar profiles were obtained from all examined cuts [see Fig. 2(b)], indicating that sequential doping for two weeks with saturated F4TCNQ solutions is not sufficient to evenly dope the solid chunks throughout the whole volume of material.

Since the F4TCNQ concentration at the center of the cube was found to be negligible, we were able to use the concentration profile of the dopant to quantify the diffusion coefficient. We approximate the diffusion of F4TCNQ into P3HT by a 1D-model. Similar to other reports,[12,16] we assumed that an equilibrium between neutral and ionized F4TCNQ exist, which can be described by

$$[P] + [F] \rightleftarrows [P^+] + [F^-], \qquad (2)$$

where [F] and [F$^-$] denote the concentration of neutral and ionized dopant molecules and [P] and [P$^+$] denote the concentration of neutral and charged polymer sites, respectively. As F4TCNQ anions are Coulombically bound to adjacent polarons, the diffusion rate of the former is expected to be much lower than that of neutral F4TCNQ molecules, as indeed observed by Moulé et al.[12] Hence, the charged dopant fraction was treated as immobile, while the diffusion of neutral F4TCNQ was modeled using a modified version of Fick's second law:

$$\frac{\partial[F]}{\partial t} = D \times \frac{\partial^2[F]}{\partial x^2} - f, \qquad (3)$$

where D is the diffusion constant, and
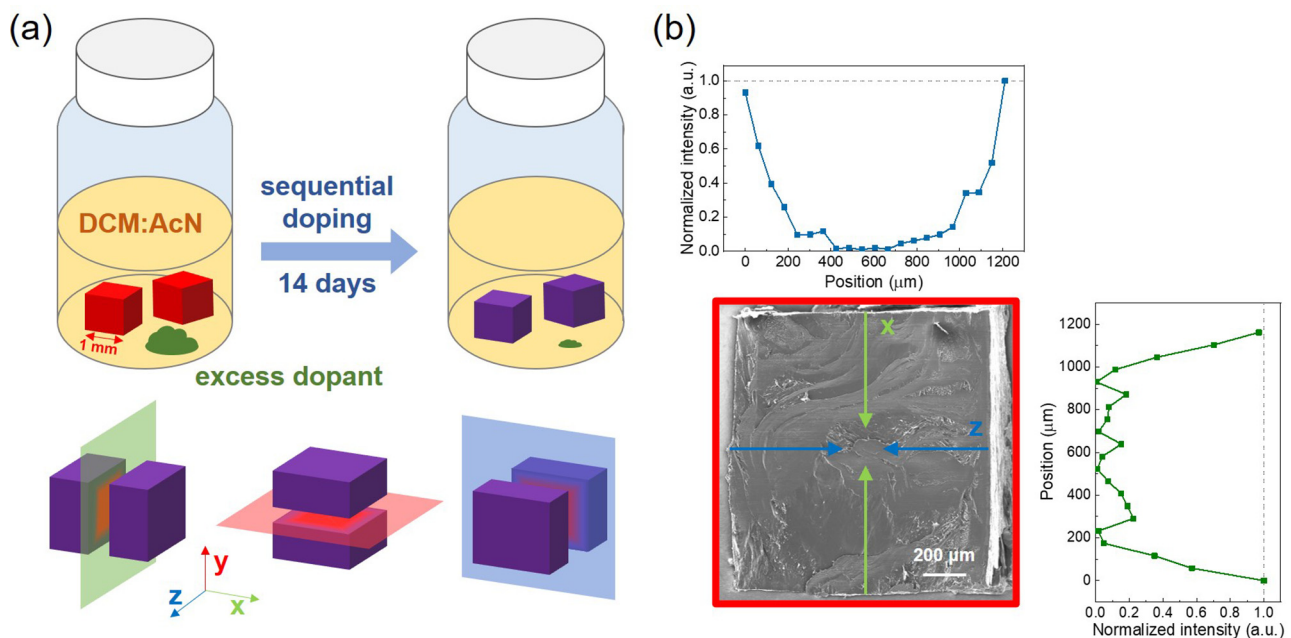
FIG. 1. (a) Schematic of the sequential doping process where pressed blocks of P3HT are placed in a saturated solution of F4TCNQ in 1:1 dichloromethane:acetonitrile (DCM:AcN), and illustrations of the cross section cuts perpendicular to the direction of flow (x), direction of applied force (y) and the third axis (z). (b) SEM image of the cross section perpendicular to the y-axis and normalized intensity of the fluorine EDX signal along the x- and z-axes.
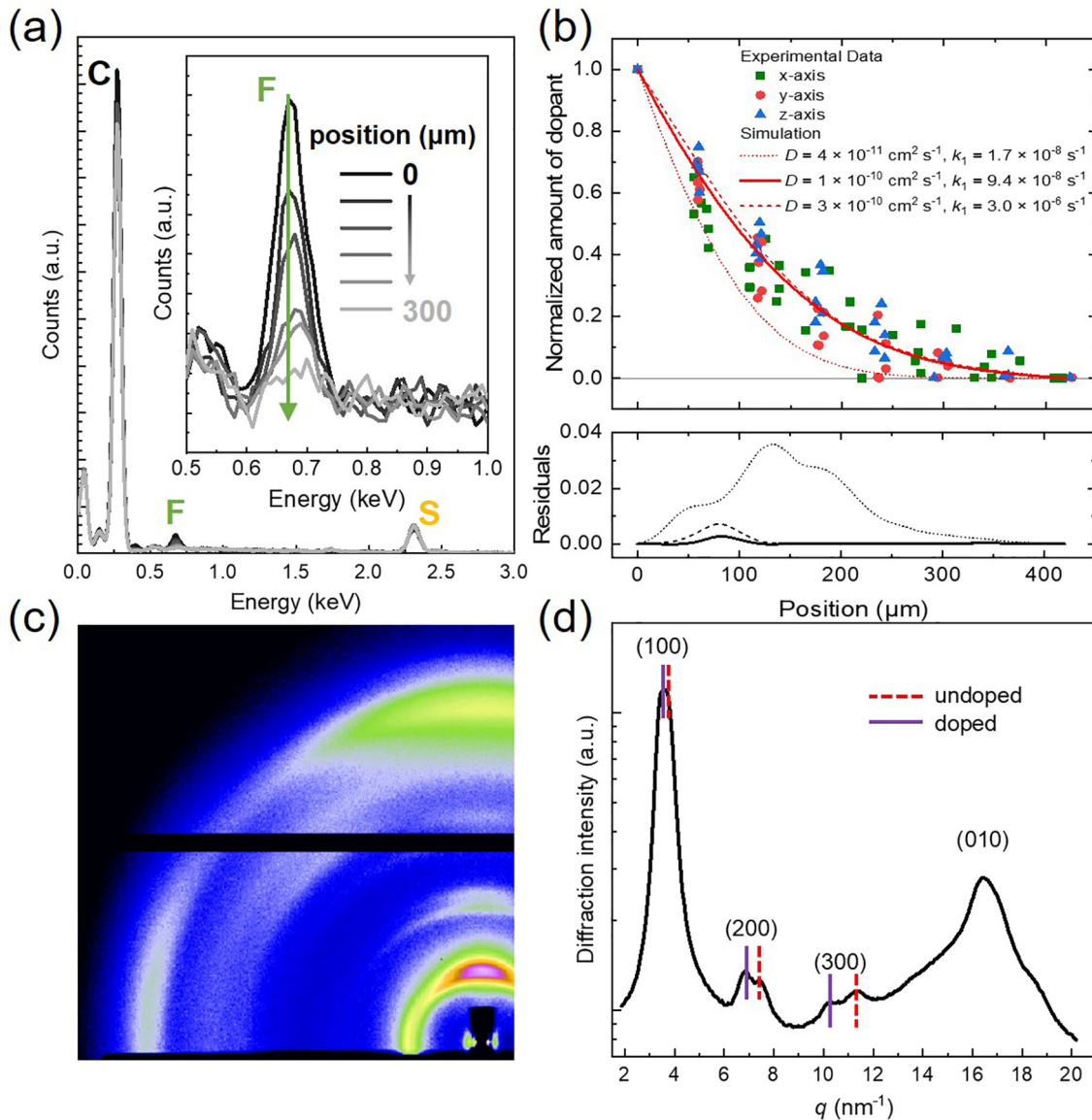
FIG. 2. (a) EDX spectra obtained at various positions along the x-axis on the cross section (normal to the y-axis); highlighted signals correspond to carbon, fluorine, and sulfur atoms; insert = fluorine signal recorded at various positions away from the cube surface. (b) Normalized intensity of the EDX fluorine signal (symbols) as a function of distance from the cube surface along the x-, y-, and z-axes, and simulated F4TCNQ concentration profile (lines) with sum of residuals (χ^2) plotted for different combinations of the diffusion coefficient (D) and rate constant (k_1). (c) WAXS image of the block taken in transmission parallel to the z-axis and (d) integrated diffractogram from the same image.

$$f = \frac{\partial[\text{F}^-]}{\partial t} = k_1[\text{F}][\text{P}] - k_2[\text{P}^+][\text{F}^-], \qquad (4)$$

where k_1 and k_2 are the rate constants of the reaction described in Eq. (2). As the second term of Eq. (4) is significantly smaller than the first, it is neglected here. Equation (3) is solved stepwise using a forward Euler scheme with a diffusion current set to zero at the surface of the cube. The extracted parameters D and k_1 correspond to the combination for which the lowest sum of residuals χ^2 was identified [Figs. 2(b) and S1]. To illustrate the best fit for D and k_1, doping profiles for different combinations of D and k_1 were generated [Fig. 2(b)].

The diffusion profiles inferred from the intensity of the EDX fluorine signal along the x-, y-, and z-axes were remarkably similar [Fig. 2(b)]. As a result, our simulations yield a similar diffusion coefficient for F4TCNQ of $D \sim 10^{-10}$ cm^2 s^{-1} along all three axes. Considering the spread of the EDX data, we conclude that there is no significant difference for dopant entering the polymer parallel or perpendicular to the flow direction, the latter of which corresponds to the preferred orientation direction of the polymer backbone.[15]

A wide-angle x-ray scattering [WAXS, Fig. 2(c)] image recorded in transmission along the z-axis and the integrated diffractogram of

TABLE I. Thermoelectric properties of sequentially doped P3HT cubes: electrical conductivity σ, Seebeck coefficient α, thermal conductivity κ, power factor $\alpha^2\sigma$, and figure of merit zT.

Axis	σ (S cm^{-1})	α (μV K^{-1})	κ (W m^{-1} K^{-1})	$\alpha^2\sigma$ (μW m^{-1} K^{-2})	zT (10^{-4})
x	2.2 ± 0.2	42 ± 2	0.58 ± 0.01	0.39 ± 0.04	2.0 ± 0.2
y	0.3 ± 0.1	47 ± 3	0.40 ± 0.02	0.06 ± 0.02	0.4 ± 0.1
z	0.8 ± 0.1	46 ± 4	0.59 ± 0.04	0.16 ± 0.03	0.8 ± 0.2

the same image [Fig. 2(d)] show distinct $h00$ scattering peaks ($h = 1$–3) due to lamellar stacking as well as a 010 peak due to π-stacking. We conclude that crystalline domains were aligned with the polymer backbone oriented along the flow direction (x-axis) and the side chains with preferential orientation along the load direction (y-axis). The invariance of D despite the presence of ordered crystalline domains likely arises because dopant molecules predominantly diffuse through amorphous regions.[17] The $h00$ scattering peaks were split,
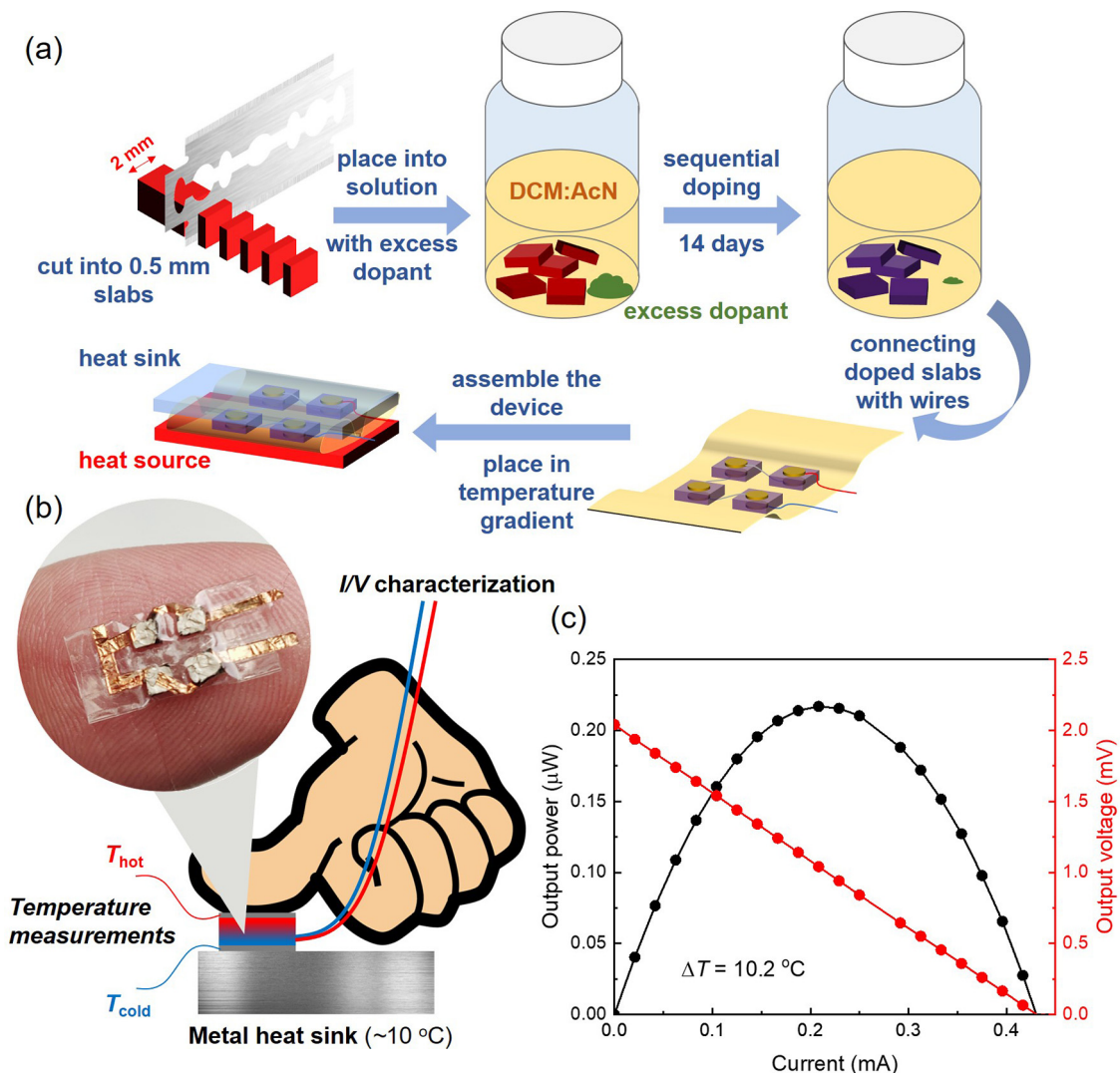
FIG. 3. (a) Schematic illustration of the fabrication procedure of the thermoelectric module. (b) Illustration of the setup to characterize a 4-leg thermoelectric module; inset = photograph of the module on the first author's left thumb. (c) Output power generated for different load currents at a temperature difference of $\Delta T = 10.2\,^\circ$C across the module (measured with two thermocouples) generated by placing the module between a cold metal surface ($\sim$10 $^\circ$C) and one of the thumbs of the first author.

which confirms the presence of both undoped and doped material. Intercalation of F4TCNQ between the side chains of P3HT increases the distance between adjacent polymer backbones along the lamellar stacking direction, which results in a shift of the $h00$ scattering peaks to lower q-values.[8,10,18] We argue that the F4TCNQ molecules that are intercalated between the side chains of P3HT are predominately ionized and, hence, less mobile (cf. discussion above).

In a further set of experiments, we characterized the thermoelectric properties of sequentially doped cubes of P3HT (Table I). The cubes feature significant anisotropy in terms of electrical conductivity with values of $\sigma \sim 2.2$, 0.3, and 0.8 S cm^{-1} measured along the x-, y-, and z-axes, respectively, calculated according to

$$\sigma = \frac{1}{R} \cdot \frac{L}{A}, \quad (5)$$

where R is the measured electrical resistance, $L = 1$ mm and $A = 1 \times 1$ mm^2 are the thickness and cross-sectional area of the doped cube. We explain the higher electrical conductivity along the flow direction with the alignment of crystalline domains, which enhances the charge–carrier mobility, as also observed for oriented thin films[19–21] and stretched P3HT.[22] The Seebeck coefficient did not display any appreciable anisotropy (see Table I). In the case of the thermal conductivity, calculated according to $\kappa = \rho \cdot c_p \cdot \delta$, where δ is the thermal diffusivity, we observed higher values along the x- and z-axes, e.g., $\kappa \sim 0.58$ W m^{-1} K^{-1} along the flow direction. This value is higher than values of 0.2 to 0.3 W m^{-1} K^{-1} reported for undoped P3HT.[23,24] Since the electronic contribution to κ is found to be negligible for $\sigma < 10$ S cm^{-1},[25] we rationalize the measured values with the high structural order of the here investigated P3HT cubes. We obtain the highest power factor $\alpha^2\sigma \sim 0.39\,\mu$W m^{-1} K^{-2} and figure of merit $zT \sim 2 \times 10^{-4}$ along the x-axis, which is comparable to previously reported values for F4TCNQ-doped P3HT bulk samples.[26]

We constructed a 4-leg thermoelectric module by cutting a pressed block of P3HT with dimensions of $2 \times 2 \times 2$ mm^3 into slabs ($0.5 \times 2 \times 2$ mm^3) parallel to the y-axis [Fig. 3(a)]. These slabs were sequentially doped with F4TCNQ for 14 days, placed onto the glue side of a section of scotch tape and finally connected with copper wires (see Fig. 3). The module was sealed by folding the two sides of the scotch tape inward [Fig. 3(a)] and had a total internal resistance of $R_{in} = 4.6\,\Omega$. The module was placed between a cold metal surface ($\sim 10\,°$C) and a thumb of the first author, which provided a temperature gradient of $\Delta T = 10.2\,°$C across the module, measured by placing two thin-film thermocouples on either side. The gentle downward force (<10 N) applied by the thumb reduced thermal contact resistance as much as possible without deforming the module. We estimate that the thumb exerted a force of about 10 N.

We measured an open-circuit voltage of $V_{oc} = 2.0$ mV, which is in good agreement with a value of 1.7 mV predicted according to

$$V_{oc} = (\alpha - \alpha_{Cu}) \cdot \Delta T \cdot n, \quad (6)$$

where $\alpha_{Cu} = 1.9\,\mu$V K^{-1} is the Seebeck coefficient of copper and n is the number of the legs. The output power reached a maximum of $P_{out} = 0.22\,\mu$W at load matching conditions, which is in agreement with a value of $0.23\,\mu$W predicted according to

$$P_{out} = \frac{V_{oc}^2}{4R_{in}}. \quad (7)$$

In summary, we explored sequential doping of chunks of pressed P3HT with F4TCNQ by sequential doping for two weeks. The dopant is found to ingress into the solid material with a diffusion coefficient of 10^{-10} cm^2 s^{-1} at room temperature, resulting in a doping gradient with a 250 μm thick doped surface layer and an undoped interior. The highest electrical conductivity of 2.2 S cm^{-1} was measured along the flow direction resulting in a power factor of $0.39\,\mu$W m^{-1} K^{-2}. Solid slabs of doped P3HT could be arranged into a 4-leg thermoelectric module that generated a power of $0.22\,\mu$W when pressing a thumb onto the device.

See the supplementary material for the experimental section and the sum of residuals obtained when fitting the diffusion profile with different combinations of the diffusion coefficient and rate constant.

AUTHOR DECLARATIONS

Conflict of Interest

The authors have no conflicts to disclose.

DATA AVAILABILITY

Data that support the findings of this study are available from the corresponding authors upon reasonable request.

REFERENCES

[1]Q. Zhang, Y. Sun, W. Xu, and D. Zhu, Adv. Mater. **26**, 6829 (2014).
[2]O. Bubnova and X. Crispin, Energy Environ. Sci. **5**, 9345 (2012).
[3]M. Campoy-Quiles, Philos. Trans. R. Soc., A **377**, 20180352 (2019).
[4]B. Russ, A. Glaudell, J. J. Urban, M. L. Chabinyc, and R. A. Segalman, Nat. Rev. Mater. **1**, 16050 (2016).
[5]M. Lindorf, K. A. Mazzio, J. Pflaum, K. Nielsch, W. Brütting, and M. Albrecht, J. Mater. Chem. A **8**, 7495 (2020).
[6]R. Kroon, D. A. Mengistie, D. Kiefer, J. Hynynen, J. D. Ryan, L. Yu, and C. Müller, Chem. Soc. Rev. **45**, 6147 (2016).
[7]I. E. Jacobs, E. W. Aasen, J. L. Oliveira, T. N. Fonseca, J. D. Roehling, J. Li, G. Zhang, M. P. Augustine, M. Mascal, and A. J. Moulé, J. Mater. Chem. C **4**, 3454 (2016).
[8]D. T. Scholes, S. A. Hawks, P. Y. Yee, H. Wu, J. R. Lindemuth, S. H. Tolbert, and B. J. Schwartz, J. Phys. Chem. Lett. **6**, 4786 (2015).
[9]S. N. Patel, A. M. Glaudell, K. A. Peterson, E. M. Thomas, K. A. O'Hara, E. Lim, and M. L. Chabinyc, Sci. Adv. **3**, e1700434 (2017).
[10]J. Hynynen, D. Kiefer, L. Yu, R. Kroon, R. Munir, A. Amassian, M. Kemerink, and C. Müller, Macromolecules **50**, 8140 (2017).
[11]V. Vijayakumar, Y. Zhong, V. Untilova, M. Bahri, L. Herrmann, L. Biniek, N. Leclerc, and M. Brinkmann, Adv. Energy Mater. **9**, 1900266 (2019).
[12]J. Li, C. Koshnick, S. O. Diallo, S. Ackling, D. M. Huang, I. E. Jacobs, T. F. Harrelson, K. Hong, G. Zhang, J. Beckett, M. Mascal, and A. J. Moulé, Macromolecules **50**, 5476 (2017).

[13] V. Vijayakumar, E. Zaborova, L. Biniek, H. Zeng, L. Herrmann, A. Carvalho, O. Boyron, N. Leclerc, and M. Brinkmann, ACS Appl. Mater. Interfaces **11**, 4942 (2019).

[14] A. Lund, Y. Tian, S. Darabi, and C. Müller, J. Power Sources **480**, 228836 (2020).

[15] M. A. Baklar, F. Koch, A. Kumar, E. B. Domingo, M. Campoy-Quiles, K. Feldman, L. Yu, P. Wobkenberg, J. Ball, R. M. Wilson, I. McCulloch, T. Kreouzis, M. Heeney, T. Anthopoulos, P. Smith, and N. Stingelin, Adv. Mater. **22**, 3942 (2010).

[16] Y. Kim, S. Chung, K. Cho, D. Harkin, W.-T. Hwang, D. Yoo, J.-K. Kim, W. Lee, Y. Song, H. Ahn, Y. Hong, H. Sirringhaus, K. Kang, and T. Lee, Adv. Mater. **31**, 1806697 (2019).

[17] P. Y. Yee, D. T. Scholes, B. J. Schwartz, and S. H. Tolbert, J. Phys. Chem. Lett. **10**, 4929 (2019).

[18] D. T. Duong, C. Wang, E. Antono, M. F. Toney, and A. Salleo, Org. Electron. **14**, 1330 (2013).

[19] S. Qu, Q. Yao, L. Wang, Z. Chen, K. Xu, H. Zeng, W. Shi, T. Zhang, C. Uher, and L. Chen, NPG Asia Mater. **8**, e292 (2016).

[20] V. Untilova, T. Biskup, L. Biniek, V. Vijayakumar, and M. Brinkmann, Macromolecules **53**, 2441 (2020).

[21] V. Untilova, J. Hynynen, A. I. Hofmann, D. Scheunemann, Y. Zhang, S. Barlow, M. Kemerink, S. R. Marder, L. Biniek, C. Müller, and M. Brinkmann, Macromolecules **53**, 6314 (2020).

[22] J. Hynynen, E. Järsvall, R. Kroon, Y. Zhang, S. Barlow, S. R. Marder, M. Kemerink, A. Lund, and C. Müller, ACS Macro Lett. **8**, 70 (2019).

[23] C. Bounioux, P. Díaz-Chao, M. Campoy-Quiles, M. S. Martín-González, A. R. Goñi, R. Yerushalmi-Rozen, and C. Müller, Energy Environ. Sci. **6**, 918 (2013).

[24] D. Kiefer, L. Yu, E. Fransson, A. Gómez, D. Primetzhofer, A. Amassian, M. Campoy-Quiles, and C. Müller, Adv. Sci. **4**, 1600203 (2017).

[25] D. Scheunemann and M. Kemerink, Phys. Rev. B **101**, 075206 (2020).

[26] R. Kroon, J. D. Ryan, D. Kiefer, L. Yu, J. Hynynen, E. Olsson, and C. Müller, Adv. Funct. Mater. **27**, 1704183 (2017).